but because Γ is small, it is not surprising that there is a close connection between the dynamics of the dissipative system and the Hamiltonian system obtained when $\Gamma = 0$. Every frequency-locked orbit evolves smoothly as $\Gamma \rightarrow 0$ to a stable, periodic orbit of the Hamiltonian system. In fact, increasing the damping destabilizes the periodic orbits; in each case there exists a maximum value of Γ above which the orbit becomes unstable. As a general rule, the orbits (Fig. 2) that become unstable at small values of Γ are those that extend over small ranges of q; they also tend to have large periods. We therefore consider $N(\delta q)$, the total number of periodic solutions that are stable over a range of greater than δq, as a function of δq, for three values of Γ (Fig. 3). One sees that the orbits with δq less than about $\Gamma/10$ are destroyed. A similar instance of the destruction of multistable, periodic orbits by dissipation has also been reported for a system of two coupled Van der Pol oscillators (*16*).

The scaling of $N(\delta q)$ with q (Fig. 3) suggests that in the limit $\Gamma \rightarrow 0$ there are an infinite number of periodic orbits, stable over small ranges of q according to a power law

$$N(\delta q) = \delta q^{-\gamma} \quad (3)$$

A similar power-law dependence is observed for one-dimensional circle maps at the critical value of the nonlinearity, in which case γ is the fractal dimension of the "devil's staircase" of frequency-locked states (*12*). Unfortunately, our computational resources do not allow us to locate enough periodic orbits to see whether their distribution in q is self-similar. The exponent γ can be extracted by linear regression of the points with $\Gamma = 1 \times 10^{-3}$. The value of N for $\delta q = 1 \times 10^{-4}$ is probably depressed by damping and because the search for periodic orbits was limited to periods no greater than 100 trap cycles. Excluding this point gives $\gamma = 1.02 \pm 0.05$ (correlation coefficient $r = 0.997$), distinctly different from the universal value of 0.87 seen in circle maps at criticality.

The well-known ion crystals seen in Paul traps are thus seen to be the most stable members of a much larger class of frequency-locked states. The underlying Hamiltonian dynamics exhibits an apparently infinite number of stable, periodic orbits with winding numbers that are rational approximants of the secular frequencies associated with the Mathieu functions for the same parameter values. With increasing dissipation, the complicated phase space structure of the Hamiltonian system becomes progressively simpler. For infinitesimal damping, the stable, periodic orbits correspond to frequency-locked attractors; then as the dissipation increases, the attractors are gradually destroyed until, for sufficiently large damping, only the crystal remains.

REFERENCES AND NOTES

1. W. Neuhauser, M. Hohenstatt, P. Toschek, H. Dehmelt, *Phys. Rev. Lett.* **41**, 233 (1978).
2. R. F. Wuerker, H. Shelton, R. V. Langmuir, *J. Appl. Phys.* **30**, 342 (1959).
3. F. Diedrich, E. Peik, J. M. Chen, W. Quint, H. Walther, *Phys. Rev. Lett.* **59**, 2931 (1987).
4. D. J. Wineland, J. C. Bergquist, W. M. Itano, J. J. Bollinger, C. H. Manney, *ibid.*, p. 2935.
5. J. Hoffnagle, R. G. DeVoe, L. Reyna, R. G. Brewer, *ibid.* **61**, 255 (1988).
6. R. Blümel *et al.*, *Nature* **334**, 309 (1988).
7. R. Blümel, C. Kappler, W. Quint, H. Walther, *Phys. Rev. A* **40**, 808 (1989).
8. R. G. Brewer, J. Hoffnagle, R. G. DeVoe, *Phys. Rev. Lett.* **65**, 2619 (1990).
9. _____, L. Reyna, W. Henshaw, *Nature* **344**, 305 (1990).
10. W. M. Kaula, *An Introduction to Planetary Physics* (Wiley, New York, 1968).
11. M. Abramowitz and I. A. Stegun, *Handbook of Mathematical Functions* (Government Printing Office, Washington, DC, 1968).
12. M. H. Jensen, P. Bak, T. Bohr, *Phys. Rev. A* **30**, 1960 (1984).
13. J. Hoffnagle and R. G. Brewer, *Phys. Rev. Lett.* **71**, 1828 (1993).
14. N. H. Press, B. P. Flannery, S. A. Teukolsky, W. T. Vetterling, *Numerical Recipes* (Cambridge Univ. Press, Cambridge, 1987).
15. J. A. Yorke, *Dynamics* (Univ. of Maryland, College Park, MD, 1990). Available from the author on request.
16. P. M. Battelino, C. Grebogi, E. Ott, J. A. Yorke, E. D. Yorke, *Physica D* **32**, 296 (1988).

1 March 1994; accepted 18 May 1994

Surface Pinning as a Determinant of the Bulk Flux-Line Lattice Structure in Copper Oxide Superconductors

Seokwon Yoon, Hongjie Dai, Jie Liu, Charles M. Lieber*

Direct knowledge of crystal defects and their perturbation of magnetic flux lines is essential to understanding pinning and to devising approaches that enhance critical currents in superconductors with high critical temperatures (T_c). Atomic force microscopy was used to simultaneously characterize crystal defects and the magnetic flux-line lattice in single crystals of $Bi_2Sr_2CaCu_2O_8$. Images show that surface defects, which are present on all real samples, pin the flux-line lattice. Above a critical height, the pinning interaction is sufficiently strong to form grain boundaries in the bulk flux-line lattice. These results elucidate the structure of the defects that pin flux lines and demonstrate that surface pinning, through the formation of grain boundaries, can determine the bulk flux-line lattice structure in high-T_c materials. The implications of these results to the bulk flux-line lattice structure observed in previous experiments and to enhancing critical currents are discussed.

Understanding the structure and pinning of the magnetic flux-line lattice (FLL) in the high-T_c copper oxide superconductors is a challenging problem of central importance to many applications proposed for these materials (*1*). Two techniques, neutron diffraction (*2–4*) and Bitter decoration (*5–9*), have been used to probe the structure of the FLL in the copper oxide materials. Neutron scattering experiments probe the FLL of the bulk material but, as in any diffraction experiment, cannot provide microscopic details of the FLL (for example, topological defects). Furthermore, neutron diffraction experiments have not provided direct information about crystalline defects that might pin the FLL. On the other hand, Bitter patterns, which are produced when individual flux lines are decorated with small magnetic particles as they emerge from the surface of a superconductor, can be used to address directly the microscopic structure of the FLL. This microscopic view has led to the identification of several structures, including a hexatic glass (*6*), a chain state (*7, 8*), and grain boundaries (*9*).

The conventional Bitter decoration technique is limited in several respects. It is implicitly assumed that the surface structure probed by this technique is representative of the bulk FLL. This assumption has been questioned theoretically (*10*) because the flux lines in the copper oxide materials have both a large line energy, which makes them susceptible to pinning by surface roughness, and a small line tension, which makes them flexible. Hence, flux lines pinned by surface defects could bend and adopt a different structure in the bulk. There is some experimental evidence from Bitter patterns for pinning of the FLL by surface roughness (*9*); however, it is still unclear whether the FLL seen at the surface is the same or differs from that of the bulk. This situation is not surprising because the techniques used to view the patterns, electron or optical microscopy, provide little quantitative infor-

Division of Applied Sciences and Department of Chemistry, Harvard University, Cambridge, MA 02138, USA.

*To whom correspondence should be addressed.

mation about the crystal defects that might be pinning flux lines. In this regard, Bitter decoration and neutron diffraction are both limited.

Direct knowledge of these defects and of how they perturb flux lines is needed for a quantitative understanding of FLL pinning and in efforts to enhance critical currents in the high-T_c materials. To this end, we report atomic force microscopy (AFM) studies of Bitter patterns on single crystals of $Bi_2Sr_2CaCu_2O_{8+\delta}$ (BSCCO) that quantitatively and simultaneously characterize the structure of surface defects and the FLL. We show that surface steps, which are present on all real samples, pin flux lines. Measurements made as a function of step height demonstrate that above a critical height, the pinning interaction is sufficiently strong to form grain boundaries in the bulk FLL. In addition, pinning by other defects, including bent crystal surfaces and surface cracks, have been characterized. These results may shed light on the bulk FLL structure observed in previous experiments (*2*, *3*) and on ways to enhance critical currents.

Single crystals of BSCCO were grown according to a method described elsewhere (*11*). The as-grown crystals were subsequently annealed for ~10 days in oxygen at 450°C to remove oxygen vacancies because these defects may pin the FLL. The magnetically determined transition widths (90 to 10%) of the annealed crystals were small (≤2 K) and indicate that the crystals are homogeneous and of high quality. The crystals were cleaved (typical size 2 mm by 2 mm by 0.05 mm) and cooled in a magnetic field applied parallel to the *c* axis of the crystals. After the crystals were cooled to 4.2 K, magnetic iron clusters were evaporated to decorate the flux lines emerging at the BSCCO surface. Although the decoration is carried out at 4.2 K, the resulting flux-line pattern corresponds to the position of flux lines frozen at some higher temperature (*1*, *8*, *9*). The decoration procedure has been described in detail elsewhere (*12*). After the decoration, samples were warmed to room temperature, and we recorded the Bitter pattern using an atomic force microscope or a scanning electron microscope.

A comparison of the images obtained by AFM and scanning electron microscopy (SEM) from the same decorated BSCCO sample area is shown in Fig. 1. Two distinct types of structures can be seen in these images: the magnetic FLL and surface steps. The AFM image (Fig. 1A) shows a hexagonal pattern of small light spots ~300 nm in diameter over the entire BSCCO surface. These features correspond to the positions of individual flux lines decorated with the iron clusters. In contrast, the FLL is barely visible in SEM images (Fig. 1B) of the same sample area (*13*). Generally we find that the AFM images exhibit better

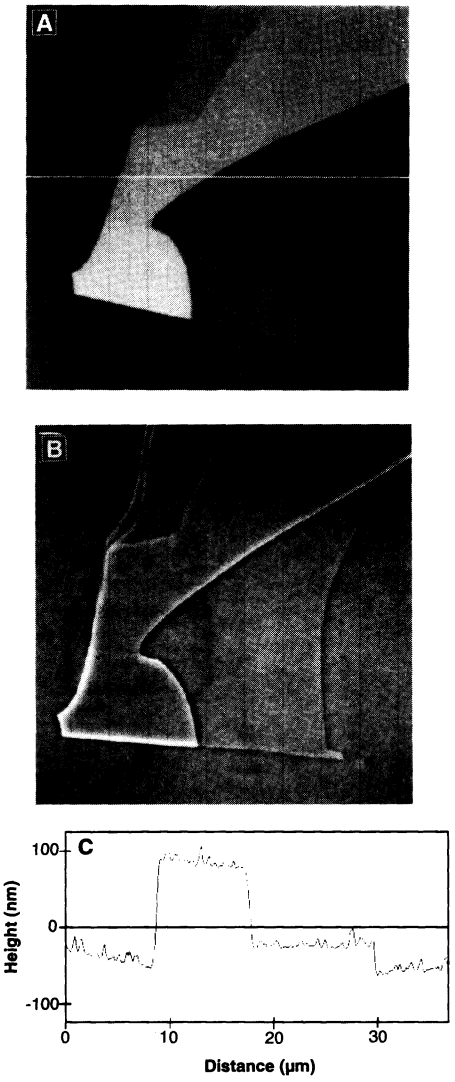

Fig. 1. (**A**) AFM and (**B**) SEM images of the same area of a BSCCO single crystal decorated at 4.2 K with iron clusters in a field of 33 G. The light circular spots in (A) correspond to the positions of flux lines at the sample surface. Each flux-line feature has a diameter of 0.3 to 0.4 μm and is composed of individual iron clusters having diameters of 20 to 30 nm. The FLL constant is 0.85 μm, and the image area is 36.9 μm by 36.9 μm. A series of surface steps is also present in the center portions of (A) and (B). We highlight quantitatively the size of these steps by plotting in (**C**) the height variation along the white line drawn across (A). The AFM images reported in this study were recorded in air with a Nanoscope III AFM using Si_3N_4 cantilevers and tips.

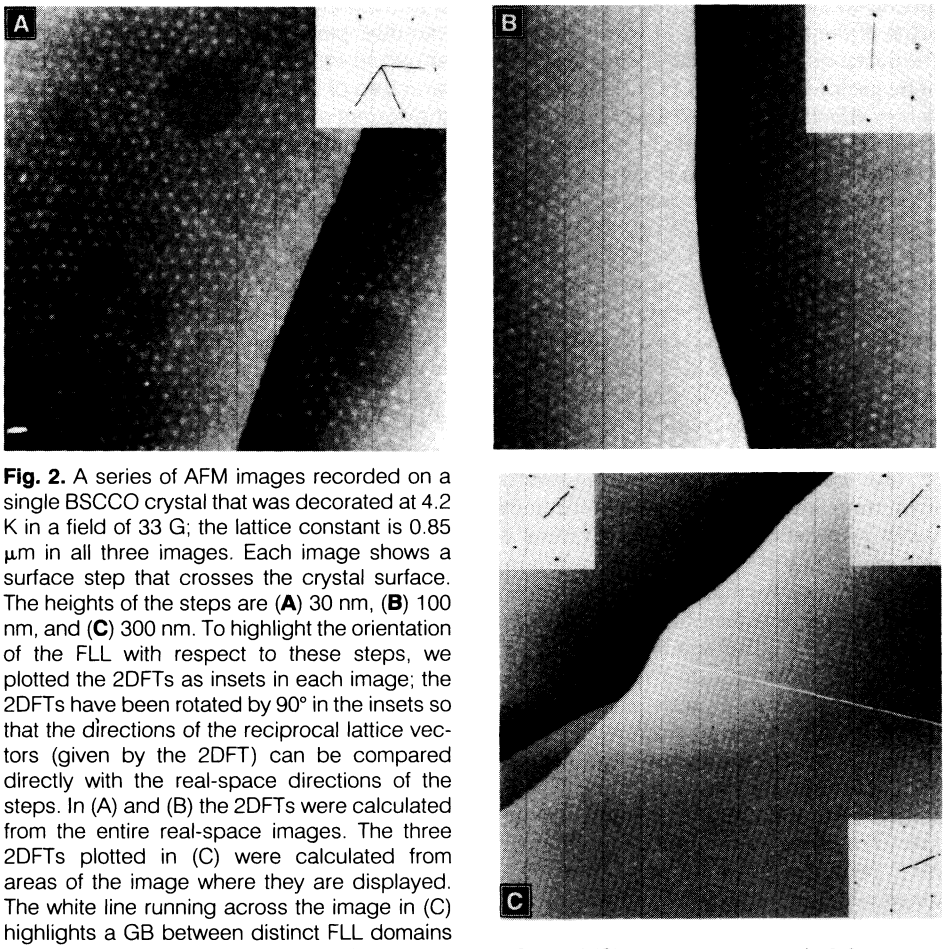

Fig. 2. A series of AFM images recorded on a single BSCCO crystal that was decorated at 4.2 K in a field of 33 G; the lattice constant is 0.85 μm in all three images. Each image shows a surface step that crosses the crystal surface. The heights of the steps are (**A**) 30 nm, (**B**) 100 nm, and (**C**) 300 nm. To highlight the orientation of the FLL with respect to these steps, we plotted the 2DFTs as insets in each image; the 2DFTs have been rotated by 90° in the insets so that the directions of the reciprocal lattice vectors (given by the 2DFT) can be compared directly with the real-space directions of the steps. In (A) and (B) the 2DFTs were calculated from the entire real-space images. The three 2DFTs plotted in (C) were calculated from areas of the image where they are displayed. The white line running across the image in (C) highlights a GB between distinct FLL domains at the top and bottom of the image. The images (A), (B), and (C) are 25.4, 31.5, and 49.6 μm on a side, respectively.

flux-line resolution than the SEM images because either too much or too little magnetic iron has been deposited onto the sample surfaces. Excess deposition reduces the corrugation at the position of the flux lines (*13*), and low deposition reduces the average cluster size decorating the flux lines; in both cases, the decorated flux lines are difficult to resolve by SEM. Interestingly, by using AFM to image small (≈10 nm) magnetic clusters, it may be possible to extend the upper field range accessible by the decoration technique.

In addition, both images show steps on the surface of the BSCCO crystals. Surface steps are a common feature on BSCCO samples. We believe that most of these steps, especially long, curved ones, are created as a result of the large strains induced during the process of cleaving any real crystal. Because surface steps can pin flux lines, it is essential to characterize their structural properties. In this regard, AFM images yield key information not available from SEM images; that is, the AFM provides a quantitative measure of the crystal surface topography while simultaneously imaging the FLL. This point is illustrated clearly through the analysis of the surface steps in Fig. 1. The heights of the steps determined from a cross section through the AFM image are 140, 105, and 35 nm (Fig. 1C). Information in the SEM image only allows one to say qualitatively that a given step is large or small.

We exploited the imaging capability of AFM to determine quantitatively how surface steps of different heights affect the FLL structure. Representative images of the FLL for a single BSCCO sample in the presence of surface steps with different heights are shown in Fig. 2. Analysis of the surface topography demonstrates that the step heights are 30, 100, and 300 nm in images 2A, 2B, and 2C, respectively. These data are typical of those observed in studies of roughly 20 independent crystals; that is, steps of varying heights are common on BSCCO crystal surfaces. Importantly, the FLL structure can differ significantly depending on the surface step height.

In Fig. 2A, the FLL orientation is independent of the step. This orientational independence is clearly evident from a comparison of the FLL reciprocal lattice vectors, which are shown in the two-dimensional Fourier transform power spectrum (2DFT) of the image (Fig. 2A, inset), with the step direction: None of these vectors is aligned along the direction of the step. In Fig. 2B, the 2DFT shows clearly that a principal axis of the FLL is aligned preferentially along the straight section of the step at the top of the image. This preferential alignment indicates that the FLL is pinned to the step. The overall orientation of the FLL is not perturbed, however, by the gentle curvature in the step in the lower part of the image. The structure of the FLL in the presence of the largest step is more complex and interesting (Fig. 2C). On the lower surface terrace located in the upper left of the image, the 2DFT shows that the FLL orientation is pinned to the direction of the step. The FLL in the upper right of this image (the higher surface terrace) is also pinned in this same orientation. The 2DFT demonstrates that the FLL orientation in the lower part of the image is rotated relative to the upper part. This rotation in the FLL follows the change in step direction that occurs in the lower part of the image. Because the FLL adopts two distinct orientations, a grain boundary (GB) is formed where the two domains meet. In summarizing our studies

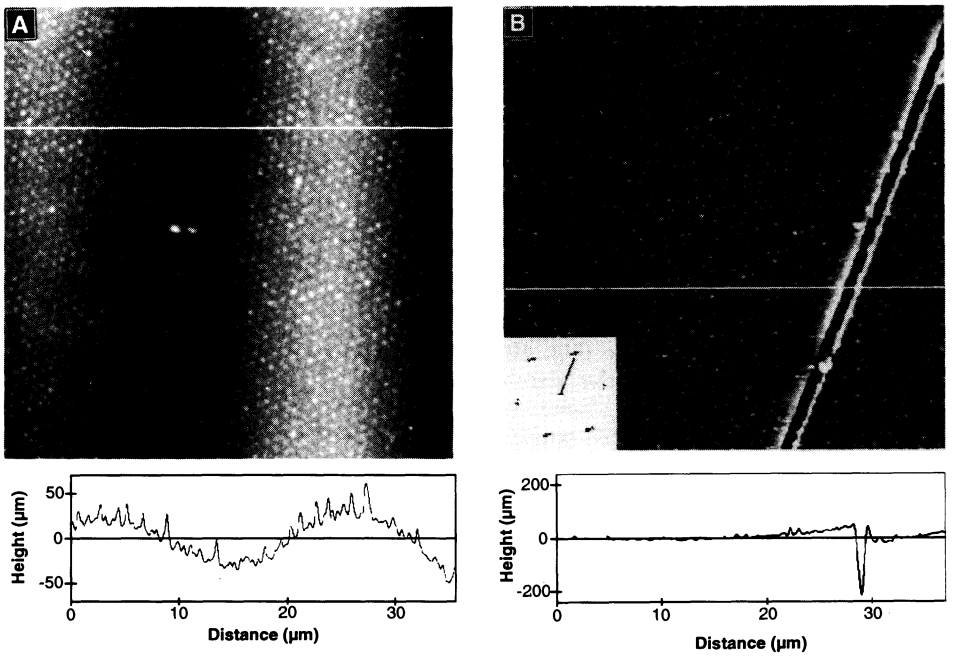

Fig. 3. AFM images of the FLL in the presence of a curved surface (**A**) and a surface crack (**B**). The crystal was decorated at 4.2 K in a field of 33 G; the FLL constant is 0.85 μm. We highlight the magnitude of the surface curvature in (A) by plotting the height variation along the white line in the image. The variation in surface topography in (B) is also shown quantitatively in a plot of the surface height along the white line in the image. The alignment of the FLL along the crack in (B) is highlighted by the 2DFT shown in the inset; the 2DFT is rotated by 90°. The images in (A) and (B) are 35.7 μm by 35.7 μm and 37 μm by 37 μm, respectively.

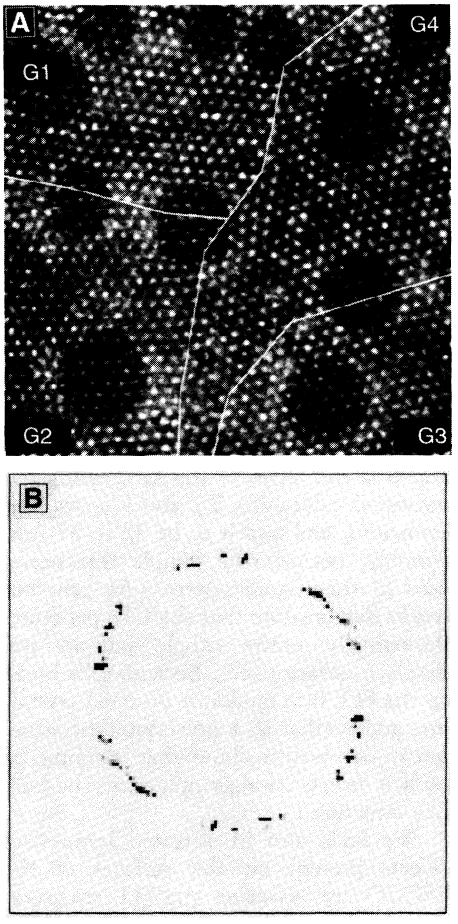

Fig. 4. (**A**) An AFM image (30 μm by 30 μm) of the FLL produced by decorating a BSCCO crystal at 4.2 K in a field of 33 G; the lattice constant is 0.85 μm. This image exhibits several FLL domains that have distinct orientations. With respect to the horizontal axis, the domains have orientations of −7°, 1°, 15°, and 23°. The GBs that form between these domains are highlighted with white lines. The large dark circles visible in the image are caused by surface contamination that occurs after the decoration process and do not affect the FLL structure. (**B**) The 2DFT calculated from the real-space image exhibits sixfold symmetry, although each of the six "peaks" has a tangential width of ~30°. The 2DFT is rotated by 90° in this plot.

of flux lines in the vicinity of surface steps, it is possible to define three regimes of pinning: (i) steps ≤30 nm in height do not affect the orientation of the FLL; (ii) steps between 30 and 200 nm in height can pin the orientation of the FLL but do not create long-range disorder in the FLL; and (iii) steps >200 nm in height pin flux lines strongly and create extended GBs in the FLL.

Quantitative analysis of the step-height dependence of GB formation provides unique insight into surface pinning and its influence on the bulk FLL properties. From our AFM data, we find that GBs with angles $\theta = 8°$ to 30° form when the step height is greater than 230 to 300 nm (*14*). These results strongly support the existence of a critical step height for GB formation. We have shown that a stable FLL GB will form when the flux-line pinning energy exceeds the energy of a GB (9). For a step of length L_s, and a GB of a length L_{GB} that extends a distance l_c perpendicular to the crystal surface, an expression for the critical step height s is given by

$$s \geq \alpha \frac{L_{GB}}{L_s} l_c$$

where

$$\alpha = \frac{\theta \ln(1/\theta)}{4\pi \ln\kappa}$$

and θ is the angle of the GB. Using our measured values of s, L_s, and L_{GB}, we can evaluate l_c and find it to be 42 to 69 μm. Notably, because the sample thicknesses used in these studies were ~50 μm, our results demonstrate that the GBs penetrate through the entire sample and are not simply a surface effect. Because GBs break up the FLL into randomly oriented crystalline grains (that is, a polycrystalline structure), our results show that pinning by surface defects strongly influences the bulk FLL structure.

We have also investigated how other defects present on the surfaces of the BSCCO crystals affect the FLL structure. Examination of the extensive set of AFM FLL images recorded in these studies shows that the cleaved BSCCO surfaces have at least two other types of defects, including curved surfaces and cracks (Fig. 3). The curved surface shown in Fig. 3A, which is typical of those observed in our studies, exhibits a peak-to-valley height change of 60 nm over a length of ~10 μm. This type of defect may be formed when crystals are mechanically dislodged from the growth melt or when they are cleaved. Analysis of the flux-line positions in the areas containing curved surfaces demonstrates that these defects do not perturb the FLL structure. The absence of pinning by curved surfaces is reasonable because there is no abrupt superconductor-vacuum interface parallel to the flux lines (the origin of pinning in the case of steps). In short, the curved surfaces locally tilt the *ab* plane of BSCCO with respect to the applied field, but because the tilt angle is small (~0.4°), there is no measurable effect on the FLL structure (*7*, *15*).

We also observe linear defects in the surface plane that penetrate into the interior of the crystals (Fig. 3B); we call these defects surface cracks. It is possible that cracks arise from imperfect growth or through severe mechanical strain. The alignment of the flux lines along the crack shown in Fig. 3B shows that these defects can strongly pin flux lines. As in the case of surface steps, the strength of flux-line pinning by cracks will depend on the distance that the crack penetrates into the crystal. The crack shown in Fig. 3B is ~250 nm in depth (*16*) and thus should be capable of forming a FLL GB. We do not observe GBs originating from cracks (linear defects do not introduce strain that can be relieved by a GB). However, FLL GBs could form in areas between two cracks or between a crack and a surface step when these defects are oriented at an angle with respect to each other (*17*).

We now consider the implications of these results. First, the formation of GBs in the FLL is significant with regard to order in the bulk FLL and to understanding the magnetic phase diagram for these materials. The analysis presented above demonstrates that FLL GBs extend through the samples, and thus, these GBs affect the bulk FLL structure. The observation of GBs over much of the BSCCO surface implies that in real samples the FLL is polycrystalline. Recognizing that the bulk FLL structure is polycrystalline is essential for properly interpreting other measurements. This point is illustrated in Fig. 4, where an image exhibiting several FLL GBs (Fig. 4A) and the 2DFT calculated from the real-space image (Fig. 4B) are shown. The 2DFT has the sixfold symmetry expected for the FLL; however, each of the six "peaks" exhibits a tangential width on the order of 30°. This large tangential width simply reflects the random orientation of FLL grains with respect to each other. Interestingly, our results provide à natural explanation for the large tangential widths of the diffraction peaks observed in a recent neutron scattering study of BSCCO (*2*). In the future it will also be important to investigate surface pinning and FLL GB formation at elevated temperatures because ultimately thermal energy may overcome the surface pinning potentials. Accounting for the temperature dependence of surface pinning and GB formation in real samples will be important to understanding intrinsic melting transitions of the FLL.

Lastly, it is interesting to consider whether surface defects can be exploited to control pinning in the high-T_c superconductors. One promising strategy would be to create defects, such as stepped surfaces, using a combination of microlithography and etching. Large surface steps will pin flux lines and could increase the critical current density (J_c), although this effect alone will not be large. However, by producing surface steps in a geometry that causes a dense, random array of FLL GBs, the enhancement in J_c could be quite large because there is a large energy associated with moving such correlated defects.

REFERENCES AND NOTES

1. D. J. Bishop, P. L. Gammel, D. A. Huse, C. A. Murray, *Science* **255**, 165 (1992).
2. R. Cubitt *et al.*, *Nature* **365**, 407 (1993).
3. M. Yethiraj *et al.*, *Phys. Rev. Lett.* **70**, 857 (1993).
4. P. L. Gammel *et al.*, *ibid.* **72**, 278 (1994).
5. G. J. Dolan, G. V. Chandrashekhar, T. R. Dinger, C. Feild, F. Holtzberg, *ibid.* **62**, 827 (1989).
6. D. G. Grier *et al.*, *ibid.* **66**, 2270 (1991).
7. C. A. Bolle *et al.*, *ibid.*, p. 112.
8. P. L. Gammel, D. J. Bishop, J. P. Rice, D. M. Ginsberg, *ibid.* **68**, 3343 (1992).
9. H. Dai, J. Liu, C. M. Lieber, *ibid.* **72**, 748 (1994).
10. D. A. Huse, *Phys. Rev. B* **46**, 8621 (1992).
11. Y. Li, J. Liu, C. M. Lieber, *Phys. Rev. Lett.* **70**, 3494 (1993).
12. R. P. Huebner, *Magnetic Flux Structures in Superconductors* (Springer-Verlag, Berlin, 1979).
13. The poor contrast in the SEM image is a result of the small variation in corrugation (10 to 20 nm) at each flux-line site, where the corrugation was determined by AFM. The small corrugations arise from the large number of magnetic clusters covering the surface and filling areas between the flux-line positions.
14. The upper and lower bounds on the step height were obtained from measurements of the minimum (maximum) step that creates (does not create) a GB. The exact height needed for GB formation cannot be determined because we rely on natural steps. Using microlithography and etching techniques to artificially control the step height could, however, provide a means for precisely determining the step height required to form a GB (S. Yoon and C. M. Lieber, unpublished results).
15. For a tilted surface the density of flux lines should be determined by the field component perpendicular to the *ab* plane: $B_\perp = B_0 \cos\theta$, where B_0 is the applied field (*7*). This relation implies that the density of flux lines will be lower on a tilted surface than on a flat one for the same applied field. Because the tilt angle is on the order of 0.4°, $B_\perp \approx B_0$ and there is no measurable effect on the density of flux lines.
16. Because the AFM tip has a finite size, this measurement provides a lower limit to the crack depth.
17. For example, consider two nearby cracks oriented at angle $\neq n \cdot 60°$ ($n = 1, 2, \ldots$). If the flux lines are strongly pinned to each of the cracks, then a GB will form between the two misoriented hexagonal FLL domains originating from the cracks.

18. We thank D. R. Nelson for helpful discussions. C.M.L. acknowledges support of this work by the National Science Foundation Division of Materials Research and the Harvard Materials Research Laboratory.

4 March 1994; accepted 18 May 1994